Supporting Information

Imidazolate framework-derived single-atom nickel catalysts for the reduction of CO_2 to CO

Yuting Li[a,b], Dandan Wang[b,c], Yuqin Ma[a,b], Fangbin Liu[a*], Hongji Li[b,c*], Qigming Xu[b*], Haijiao Xie[d]

[a] School of Chemistry and Environmental Engineering, Changchun University of Science and Technology, Changchun, Jilin, 130022, PR China

[b] Zhongshan Institute of Changchun University of Science and Technology, Zhongshan, Guangdong, 528437, PR China

[c] Hainan Engineering Research Center of Tropical Ocean Advanced Opto-electrical Functional Materials, College of Chemistry and Chemical Engineering, Hainan Normal University, Haikou, 571158, China.

[d] Hangzhou Yanqu Information Technology Co., Ltd., Hangzhou, Zhejiang, 310003, China.

1. Materials

All commercially available chemicals were not further purified unless otherwise stated. Zinc nitrate hexahydrate ($Zn(NO_3)_2·6H_2O$, 99%), nickel nitrate hexahydrate (($Ni(NO_3)_2·6H_2O$, 99%) and N,N-dimethylformamide (DMF, 99.5%) were purchased at Sinopharm Chemical Reagent Co. 2-Methylimidazole (2-MIM, 99%) and Nafion dispersion (5 wt %) were purchased at Aladdin Industrial Co. Potassium bicarbonate ($KHCO_3$, 99.5%) was purchased at Shanghai McLean Biochemical Technology Co. Methanol (99.9%) was purchased at Tianjin Aosheng Chemical Reagent Co.117 Nafion membranes were purchased from DuPont.CO_2 gas (99.999%), Ar gas (99.999%), and N_2 gas were purchased from Zhongshan City Huaxin Gas Co.

2.Synthesis of Catalyst

2.1 Synthesis of precursor Ni-ZIF-8 [1]:

2-MIM (18.27 mmol) was dissolved in methanol (25 ml) using sonication. $Zn(NO_3)_2·6H_2O$ (1.34 mmol) and $Ni(NO_3)_2·6H_2O$ (0.84 mmol) were dissolved in methanol (25 ml) and stirred for about 30 min to form a clear solution. A methanol solution containing 2-MIM was then added to the above solution and stirred at room temperature for 24 hours. After complete washing and centrifugation with DMF and methanol, respectively, the Ni molecular sieve backbone (Ni-ZIF-8) was obtained and dried under vacuum at 70℃ overnight.

ZIF-8 was obtained by not adding $Ni(NO_3)_2·6H_2O$ during the preparation.

Controls were prepared under the same experimental conditions: $Ni_{0.7}$-ZIF-$8_{(6)}$ $Ni(NO_3)_2 \cdot 6H_2O$ 0.84 mmol, 2-MIM 15.66 mmol), $Ni_{0.7}$-ZIF-$8_{(8)}$ $Ni(NO_3)_2 \cdot 6H_2O$ 0.84 mmol, 2-MIM 20.88 mmol), $Ni_{0.6}$-ZIF-$8_{(7)}$ ($Ni(NO_3)_2 \cdot 6H_2O$ 0.72 mmol, 2-MIM 18.27 mmol), $Ni_{0.8}$-ZIF-$8_{(7)}$ ($Ni(NO_3)_2 \cdot 6H_2O$ 0.96 mmol, 2-MIM 18.27 mmol).

2.2. Preparation of catalyst $Ni_{0.7}$-NC_7-1000[2]:

The prepared precursor Ni-ZIF-8 was placed in a ceramic vessel and then transferred to a vacuum tube furnace where it was pyrolysed under nitrogen at 1000℃ for 2 h at a ramping rate of 5℃/min, and then cooled to room temperature at a ramping rate of 5℃/min. The sample was then washed with distilled water and dried. The samples were transferred to 3 M H_2SO_4 for acid leaching for 12 h, and then washed with distilled water to pH neutrality to obtain Ni-N-C catalysts. The obtained N-C catalyst was dried under vacuum at 70℃ overnight.

The remaining precursors were treated in the same way for the preparation of the corresponding catalysts.

3.Characterization：

Electron micrographs were acquired via Scanning Electron Microscopy (SEM) utilizing a Hitachi SU8020 instrument (Japan), operated at an accelerating voltage of 50 kV. High-resolution Transmission Electron Microscopy (TEM), coupled with Energy Dispersive Spectroscopy (EDS) mapping, was executed on a JEOL JEM-2100F microscope set at 200 kV. High Angle Annular Dark Field Scanning Transmission Electron Microscopy (HAADF-STEM) analysis was conducted on a JEOL JEM-ARM200F system, featuring a spherical aberration corrector. Powder diffraction patterns were obtained using a Bruker AXS D8 diffractometer, equipped with Cu Kα radiation (λ=1.5418 Å). X-ray Photoelectron Spectroscopy (XPS) measurements were carried out under Ultra-High Vacuum (UHV) conditions, employing a Kratos AXIS HS monochromatized Al Kα source with a power range of 75-150 W, complemented by a low-energy electron gun for charge compensation. Differential Scanning Calorimetry-Thermogravimetric Analysis (DSC-TGA) was performed on a TA Instruments SDT Q600 analyzer. Raman spectroscopy was conducted on a Renishaw inVia spectrometer, utilizing a 532 nm laser source. Nuclear Magnetic Resonance (NMR) spectroscopy was used to quantify liquid products, employing a Bruker AVANCE AV III 600 spectrometer with deuterium oxide as the internal standard. Gas chromatography (GC) analysis, conducted on an SP-6890 instrument, was used to determine gas concentrations at 1-hour intervals during the chrono-doping process. Nitrogen adsorption isotherms were measured at 77 K using a Quantachrome Autosorb-IQ analyzer via the N_2 physisorption technique. Surface area

calculations were based on the Brunauer-Emmett-Teller (BET) method, while pore volume and size distribution were determined using the Discrete Fourier Transform (DFT) approach. Extended X-ray Absorption Fine Structure (EXAFS) data for the copper K-edge of the samples were recorded in transmission mode. Inductively Coupled Plasma-Optical Emission Spectroscopy (ICP-OES) measurements were conducted on an Agilent 5110 instrument.

4. Electrochemical measurements

Electrochemical measurements were performed using a CHI760E electrochemical workstation. The carbon dioxide reduction reaction (CO_2RR) takes place in a gas-tight H-type electrolytic cell separated by a cation-exchange membrane (Nafion 117 membrane). Each compartment of the cell contains 50 mL of 0.5 M potassium bicarbonate ($KHCO_3$) as the electrolyte. The cathode solution was purged with carbon dioxide at a rate of 20 ml/min until saturation was reached. To prepare the working electrode, 160 μL of homogeneous ink (consisting of 5 mg of sample and 50 μL of 5 wt.% Nafion solution in 950 μL of ethanol) was applied to both sides of a carbon cloth of 1 cm^2 (1 × 0.5 cm) in area, with a catalyst loading of 1 mg/cm^2. The reference electrode was a saturated calomel electrode (SCE) and the counter electrode was a platinum sheet. In carbon dioxide reduction experiments, linear scanning voltammetry (LSV) was performed in a carbon dioxide saturated electrolyte at a scan rate of 10 mV/s while stirring at 500 rpm. All LSV curves are corrected for ohmic compensation and all current densities are calculated from the geometric area of the electrodes.

Gas products are detected using a gas chromatograph (GC). Specifically, hydrogen (H_2) is measured with a thermal conductivity detector (TCD) and carbon monoxide (CO) is analyzed with a flame ionization detector (FID). Liquid products are measured using nuclear magnetic resonance (NMR) spectroscopy.

The potentials in this paper were converted to the reversible hydrogen electrode (RHE) scale by the following equation (Nernst equation at 25°C):

$$E(vs.\,RHE) = E(vs.\ Ag/AgCl) + 0.0592 * pH + 0.197$$

The farsightedness efficiency (FE) of carbon monoxide was calculated using the concentrations (ppm) detected by the gas chromatograph as follows:

$$FE = \frac{nzF}{Q} - \frac{P_0 V\%vzF}{RT_0 I_{total}} \times 100\%$$

where z=2 represents the number of electrons transferred during the reduction of carbon dioxide to a specific product, P_0 is the standard atmospheric pressure, and T_0=372.15 K is the Kelvin temperature. The flow rate of carbon dioxide used in the measurements was 20 mL/min. F is the Faraday constant with a value of 96,485 C/mol. Itotal is the total current. R is the universal gas constant with a value of 22.4 liters/mol.

Similarly, the partial current density is calculated as follows:

$$J = I \cdot FE$$

The electrochemically active surface area (ECSA) is calculated according to the following definition:

$$ECSA = C_{dl}/C_s$$

where C_{dl} corresponds to the slope of the double-layer charging current versus scan rate curve, and we used a C_s value of 40 μF cm^{-2}.

5.DFT calculations:

All computations were conducted using the Vienna Ab initio Simulation Package (VASP) with incorporated spin polarization and periodic DFT[1]. The exchange-correlation potential was handled using the generalized gradient approximation (GGA) parameterized by Perdew, Burke, and Ernzerhof (PBE)[2]. TAdditionally, the van der Waals correction from the DFT-D3 model by Grimme et al. was applied to enhance accuracy[3]. To prevent interactions between adjacent images, a vacuum layer of approximately 15 Å was incorporated. The Brillouin zone integration was carried out using a Γ-centered Monkhorst-Pack grid of 3 × 3 × 1[4], with full relaxation of the structure until the maximum force on each atom reached below 0.02 eV/Å and an energy convergence criterion of 10^-5 eV was met.

For each fundamental step, the Gibbs free energy of reaction (ΔG) was determined as the

difference between the free energies of the initial and final states. This was expressed as:

$$\Delta G = \Delta E + \Delta ZPE - T\Delta S$$

where ΔE represents the reaction energy of the reactant and product molecules adsorbed on the catalyst surface, computed via DFT; ΔZPE and ΔS denote the changes in zero-point energy and entropy, respectively, due to the reaction.

6.Supplementary Figures

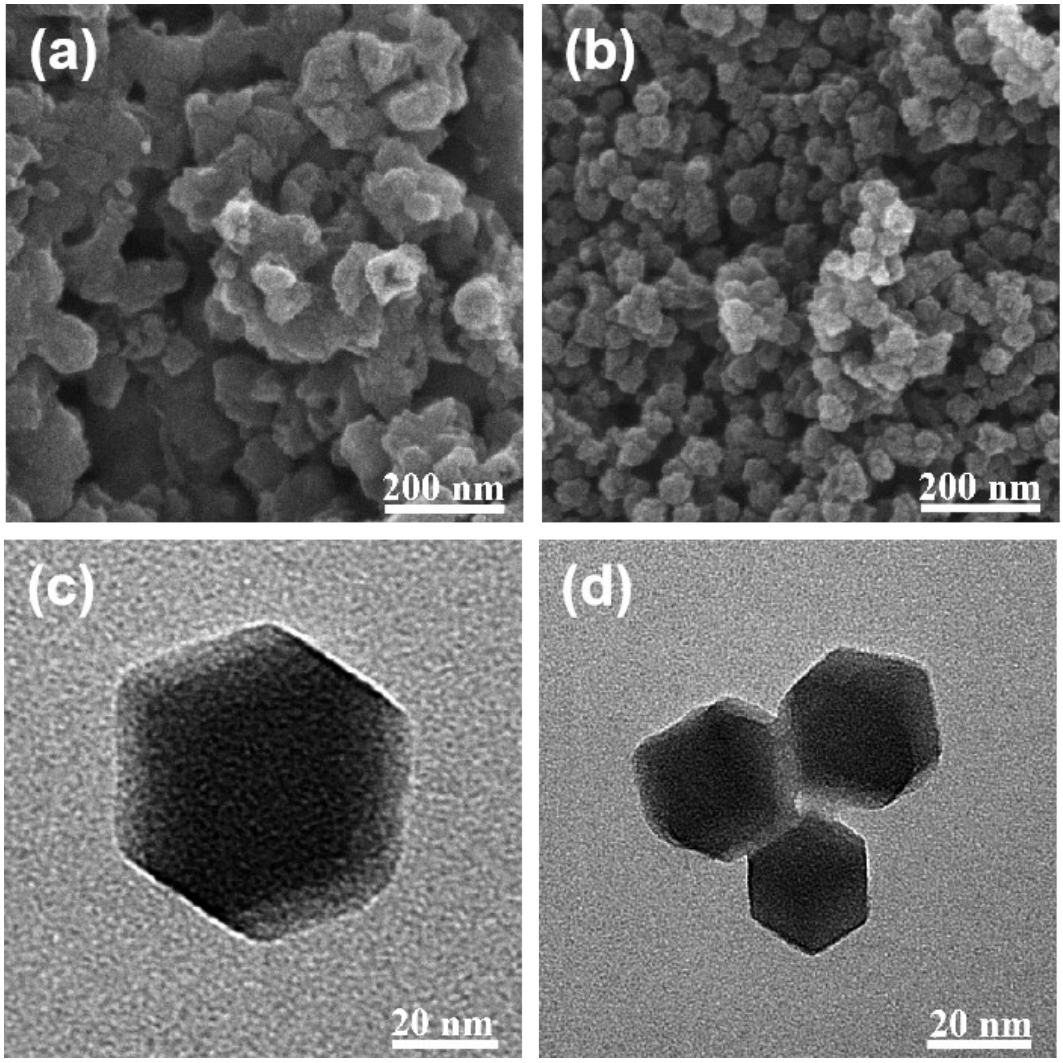

Figure S1. (a,b) SEM maps and (c,d) TEM images of ZIF-8 and Ni-ZIF-8 .

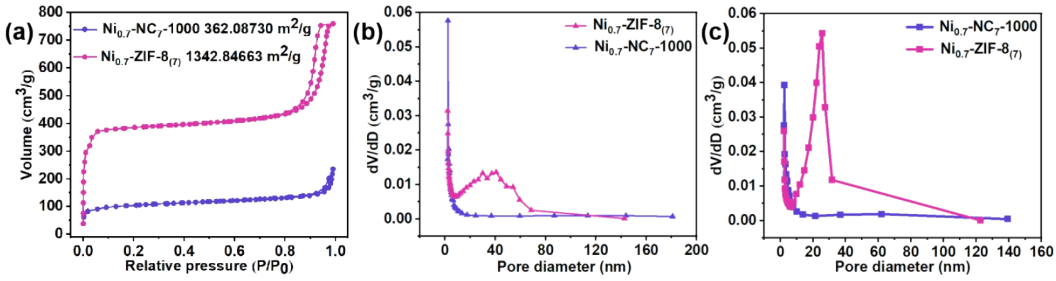

Figure S2. (a) Nitrogen adsorption-desorption isotherms and (b,c) pore size distributions of $Ni_{0.7}$-NC_7-1000 and Ni-ZIF-8.

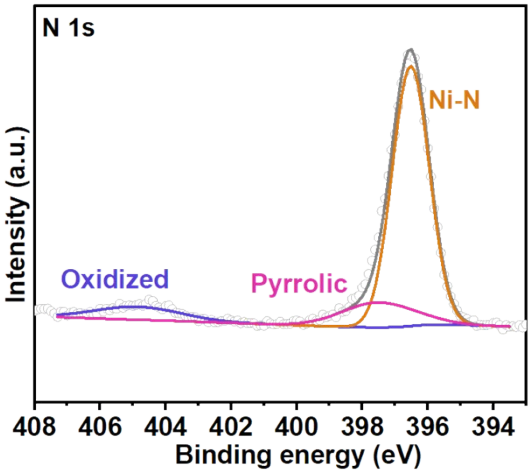

Figure S3. The N 1s XPS spectra of Ni-ZIF-8.

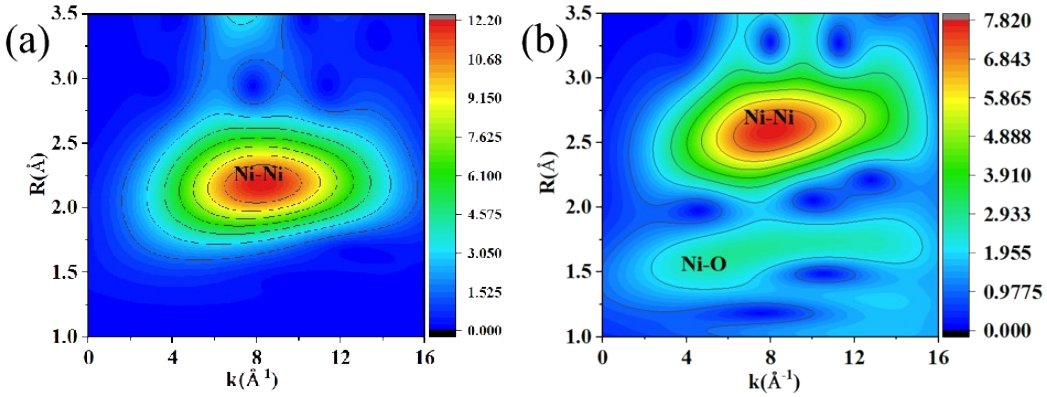

Figure S4. The WT spectra of (a) Ni foil and (b) NiO.

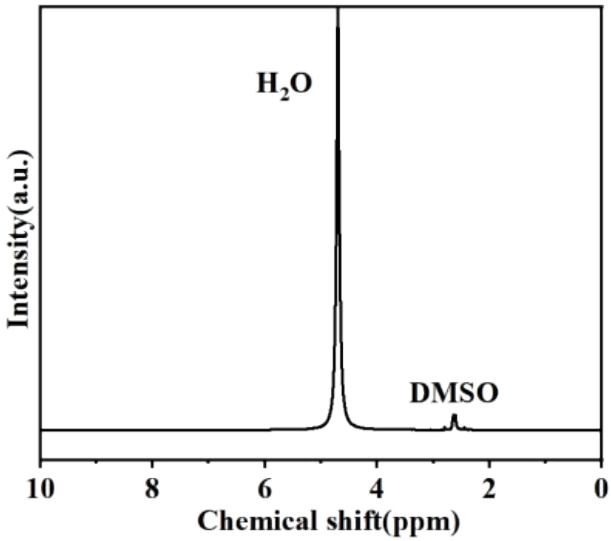

Figure S5. Characterization of liquid-phase products from electrocatalytic CO_2 reduction by Ni-

NC-1000 in CO_2-saturated 0.5 M $KHCO_3$ electrolyte at -0.88 V vs. RHE for 4 hours using ^1H NMR spectroscopy.

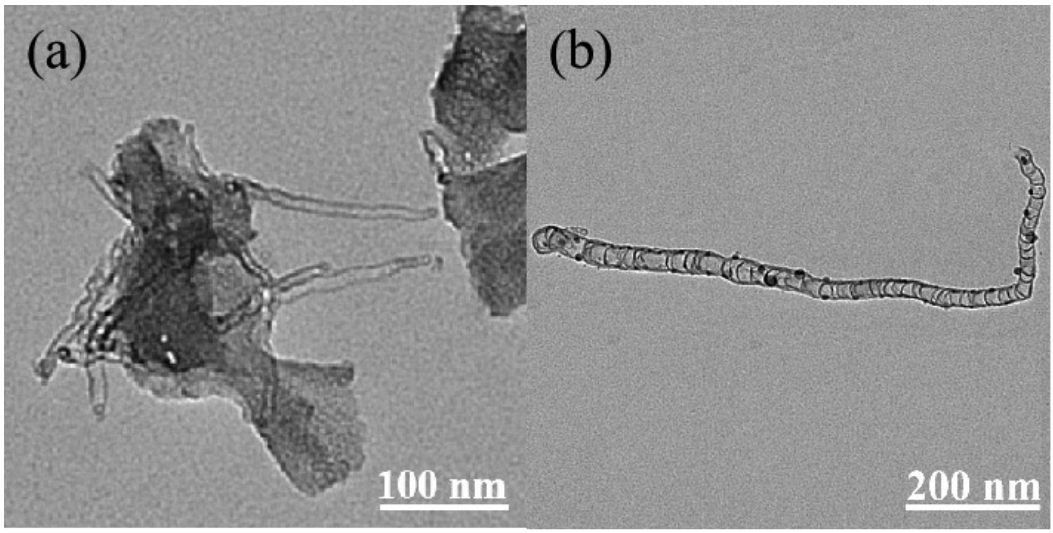

Figure S6. TEM plots of catalysts with different MIm contents.

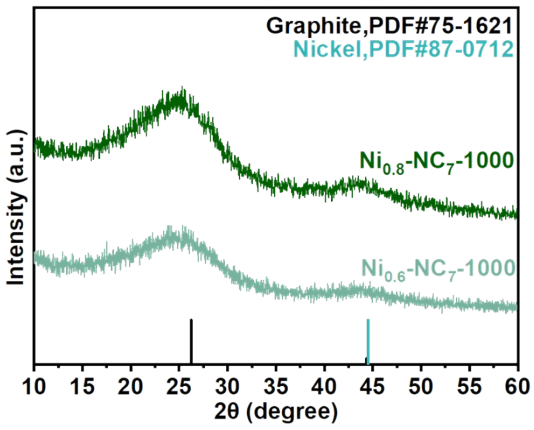

Figure S7. XRD of catalysts with different Ni^{2+} contents.

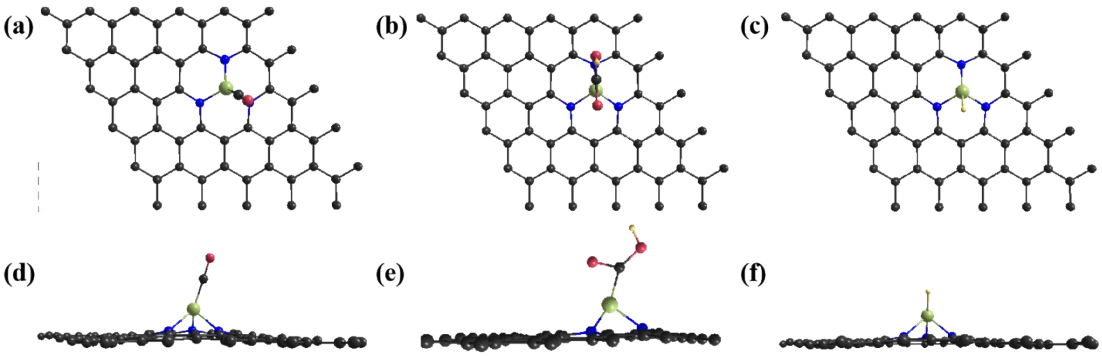

FigureS8. Geometrical configurations of the reaction intermediates *CO, *COOH and *H at the Ni-N_3 site, (a-c) top view and (d-f) side view.

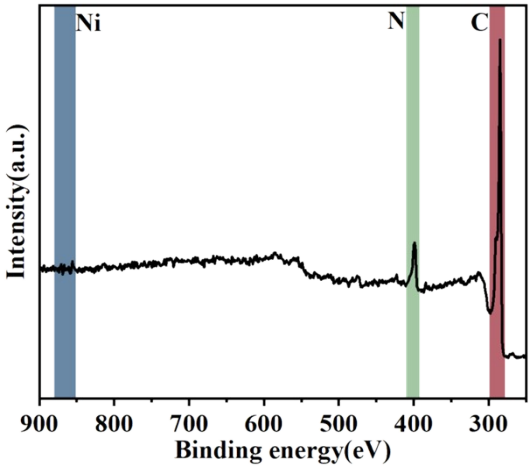

FigureS9. Full XPS spectrum of $Ni_{0.7}$-NC_7-1000.

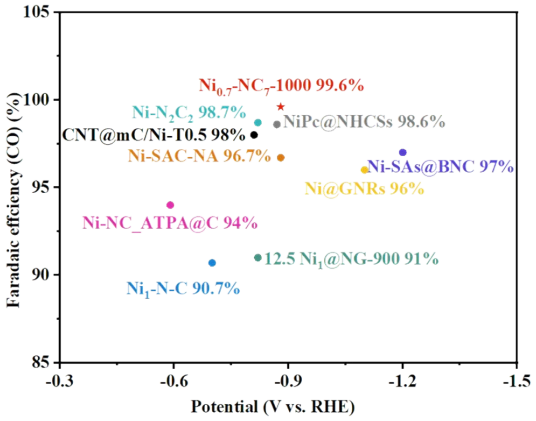

FigureS10. Compare the FE CO of different Ni-based single-atom catalysts.

7.Supplementary Tables

Table S1. Pore volumes and size distributions of the catalysts obtained from N_2 adsorption-desorption isotherms

Catalysts	S_{BET} (m^2/g)	V_{tota} (cm^3/g)	V_{mic} (cm^3/g)	V_{mes} (cm^3/g)	V_{mac} (cm^3/g)	V_{mic}/V_{tot} al (%)	V_{mes}/V_{total} (%)	V_{mac}/V_{tot} al (%)	Pore Size (nm)
Ni-ZIF-8	1341.85	1.18	0.54	0.52	0.12	45.76	44.07	10.17	3.92
Ni-NC-1000	362.09	0.36	0.12	0.13	0.11	33.33	36.11	30.56	4.30

Table S2. EXAFS fitting parameters at the Ni K-edge for various samples（S_0^2=0.98 from Ni-foil）

Sampie	Shell	*CN*[a]	*R*[b](Å)	σ^{2c}(Å^2)	$\Delta E_0{}^d$(eV)	*R* factor
Ni-foil	Ni-Ni	12	2.48±0.01	0.0077	6.6±1.0	0.0113
Ni-NC-1000	Ni-N	3.40±0.2	2.05±0.02	0.0068	2.0±1.1	0.0115

[a]*CN*: coordination numbers; [b]*R*: bond distance; [c]σ^2: Debye-Waller factors; [d] ΔE_0: the inner potential correction. R factor: goodness of fit. Error bounds that characterize the structural parameters obtained by EXAFS spectroscopy were estimated as CN±20%; R ± 1%; σ^2 ± 20%.

[1] G. Kresse, J. Furthmüller. Efficient iterative schemes for ab initio total-energy calculations using a plane-wave basis set. **Phys Rev B.** 1996, 54, 11169.

[2] J.P. Perdew, K. Burke, M. Ernzerhof. Generalized gradient approximation made simple. **Phys Rev Lett.** 1996, 77, 3865.

[3] S. Grimme, J. Antony, S. Ehrlich, H. Krieg. A consistent and accurate ab initio parametrization of density functional dispersion correction (DFT-D) for the 94 elements H-Pu. **J Chem Phys.** 2010, 132, 154104.

[4] H.J. Monkhorst, J.D. Pack. Special points for Brillouin-zone integrations. **Phys Rev B.** 1989,

13, 5188-5192.